

Self-sustained oscillations of active viscoelastic matter

Emmanuel L. C. VI M. Plan

*Institute of Theoretical and Applied Research, Duy Tan University, Ha Noi 100 000, Viet Nam and
Faculty of Natural Science, Duy Tan University, Da Nang 550 000, Viet Nam*

Huong Le Thi

Department of Mathematics and Informatics, Thang Long University, Ha Noi 100 000, Viet Nam

Julia M. Yeomans

*The Rudolf Peierls Centre for Theoretical Physics, Department of Physics, University of Oxford,
Clarendon Laboratory, Oxford OX1 3PU, United Kingdom*

Amin Doostmohammadi

The Niels Bohr Institute, University of Copenhagen, Blegdamsvej 17, 2100 Copenhagen, Denmark

Models of active nematics in biological systems normally require complexity arising from the hydrodynamics involved at the microscopic level as well as the viscoelastic nature of the system. Here we show that a minimal, space-independent, model based on the temporal alignment of active and polymeric particles provides an avenue to predict and study their coupled dynamics within the framework of dynamical systems. In particular, we examine, using analytical and numerical methods, how such a simple model can display self-sustained oscillations in an activity-driven viscoelastic shear flow.

I. INTRODUCTION

Active nematics are a class of living or synthetic materials that possess some form of orientational order and that are continuously driven by their constituent living or artificially active elements [1, 2]. The orientational order could arise from the elongated shape of the particles, such as in filamentous cytoskeletal elements [3–5], rod-like bacteria [6–8] or spindle-shaped fibroblasts [9] and neural progenitor stem cells [10], or could be an emergent feature of deformable particles such as in monolayers of epithelial cells [11, 12]. Whether it is moving bacteria or eukaryotic cells, or subcellular filaments that are put in motion by motor proteins, the common feature of all these systems is the input of energy at the particle level, that governs system-wide patterns of motion and self-organisation in the active material. While active nematic models have been indispensable in characterising various systems of active matter, their inherent complexity, that requires coupling between density, velocity, and the orientational field, still limits theoretical advances and often requires extensive numerical computations in order to obtain generic and fundamental rules of dynamical self-organisation in active matter.

To add to this complexity, most realisations of active matter do not simply exist in homogeneous and isotropic environments. Rather, the microenvironment surrounding living materials is often characterised by its own complex structure and responses that can feedback to the active matter dynamics. Prominent among these is viscoelasticity that allows living materials to constantly deform their surroundings and then to exploit the deformation and relaxation dynamics of their viscoelastic environment as an external spatio-temporal input for their own self-organisation. Examples include bacterial biofilm formation in extracellular matrices [13–15], epithelial and fibroblast cells self-propelling within interconnected networks of collagen [16–18], and subcellular filaments self-organising within the crowded environment of the cytoplasm [19, 20]. Recent theoretical and experimental studies have revealed the emergence of various forms of collective behavior for active particles suspended within - or in contact with - a viscoelastic environment. In particular, numerical models of active viscoelastic nematics [21] and active nematics in contact with viscoelastic surroundings [22] have demonstrated the impact of polymeric stresses and viscoelastic relaxation times on active nematic patterns in confined geometries and in models of cell self-propulsion and cell division. Oscillations have been shown using a full space-dependent hydrodynamic models of active matter which includes viscoelasticity [21]. Moreover, combined experiments and theory have recently shown the emergence of directional switching in bacterial collectives suspended within a viscoelastic medium and confined in circular geometries [23]. Consistent with the experiments, a simplified model that maps into a Fitzhugh-Nagumo oscillator was deduced [23].

Here we show that an alternative model of active viscoelastic matter relying only on the orientation of both active and viscoelastic components along with their respective relaxation timescales can also produce oscillatory dynamics. This model was first introduced in a recent paper [24] for active matter in contact with viscoelastic surroundings to reproduce numerical observations of the reversals of the flow field in a nematic driven by pulsatile activity. We explore the generic dynamics of this minimal, intuitive, space-independent model within the framework of dynamical systems,

and prove analytically that sustained oscillatory behaviour can arise spontaneously as an effect of the viscoelastic feedback to the active forcing. We provide a phase diagram for the emergence of the oscillations in terms of the dominant time scales of the system, and differentiate their form from sinusoidal oscillations. The equations we consider are not algebraic and cannot be naively truncated nor mapped to well-known oscillators. Also, we remark that the physics described in this work is entirely different from that seen in purely active models that oscillate [25, 26], because of the presence here of a polymeric component.

II. MODEL

Consider an active nematogen and a polymer, oriented at angles θ_n and θ_p respectively with respect to the x -axis. Then, modelling both the nematogen and the polymer as rigid rods rotating in 2D in the shear $\dot{\gamma}$ created by the active stresses and the polymer relaxation, we consider the simplified, space-independent, equations of motion (first proposed in [24])

$$\dot{\theta}_n = \dot{\gamma} \lambda_n \cos 2\theta_n - (\theta_n/t_n), \quad (1)$$

$$\dot{\theta}_p = \dot{\gamma} \lambda_p \cos 2\theta_p - (\theta_p/t_p), \quad (2)$$

$$\dot{\gamma} = \frac{\zeta}{4\nu} \sin 2\theta_n - \frac{\nu_p}{4\nu t_p} \sin 2\theta_p. \quad (3)$$

The first terms on the right-hand side of Eqs. (1) and (2) describe the nematic and polymeric response to the shear, $\dot{\gamma}$, in the limit that vorticity can be neglected. $\lambda_n, \lambda_p > 0$ are phenomenological parameters related to the aligning/tumbling properties, see for example [27]. The second terms model exponential relaxation to equilibrium, with t_n, t_p the relaxation timescales of the nematic and polymer. The shear rate, Eqn. (3), is the off-diagonal term in the stress balance $\Pi_{\text{visc}} = \Pi_{\text{active}} + \Pi_{\text{polymer}}$, where ν is the fluid viscosity and ν_p is the polymeric contribution to viscosity [24]. The dynamics of the nematogen and polymer are coupled through the shear which describes the balance between the extensile ($\zeta > 0$) stress resulting from the activity of the active nematic and the contractile stress created by the polymer relaxation.

These equations represent a simplification motivated by the full hydrodynamic model investigated numerically in [24] which showed that activity pulses in a system interacting with a viscoelastic environment can spontaneously generate flow reversals driven by the stress built up in the surrounding, passive, medium. In particular, replacing the space-dependent flow by a uniform shear results in only two dynamical variables, which allows us to fully investigate the phase space and to prove the existence of oscillations.

III. RESULTS AND DISCUSSION

We discuss the results in two steps: first we will fix the value of the polymer viscosity ν_p and then we keep the elastic modulus, i.e., the ratio of the polymer viscosity to the polymer relaxation time $A_p = \nu_p/t_p$ constant.

A. Fixed polymer viscosity ν_p

We first consider the case when polymer contribution to viscosity ν_p is fixed and the elastic modulus A_p varies inversely with t_p . Note that in the absence of activity ($\zeta = 0$) the system relaxes to the equilibrium and trivial fixed point $\theta_n = \theta_p = 0$. Moreover, for finite activity, in the limit of infinite relaxation times, only the active force dictates the shear and thus the steady-state solution is $\theta_n = \pm\pi/4, \theta_p = \pm\pi/4$. Henceforth, without losing generality we restrict our analysis of the system to the box $\Omega = [-\pi/4, \pi/4]^2$. This two-dimensional system $\boldsymbol{\theta}^T = (\theta_n, \theta_p)$ can then be written as $\dot{\boldsymbol{\theta}} = \mathbf{f}(\boldsymbol{\theta})$, with $\mathbf{f} : \mathbb{R}^2 \rightarrow \mathbb{R}^2$. By introducing the time scale of active stress generation $t_a = \nu/|\zeta|$, Eqs. (1),(2) can be expressed in terms of dimensionless numbers $T_p = t_p/t_a$ and $T_n = t_n/t_a$:

$$\begin{aligned} \dot{\theta}_n &= f_n(\theta_n, \theta_p) \\ &= \frac{1}{t_a} \left(\frac{\lambda_n}{4} \cos 2\theta_n \sin 2\theta_n - \frac{\lambda_n \nu_p}{4\nu T_p} \cos 2\theta_n \sin 2\theta_p - \frac{\theta_n}{T_n} \right), \end{aligned} \quad (4a)$$

$$\begin{aligned} \dot{\theta}_p &= f_p(\theta_n, \theta_p) \\ &= \frac{1}{t_a} \left(\frac{\lambda_p}{4} \cos 2\theta_p \sin 2\theta_n - \frac{\lambda_p \nu_p}{4\nu T_p} \cos 2\theta_p \sin 2\theta_p - \frac{\theta_p}{T_p} \right). \end{aligned} \quad (4b)$$

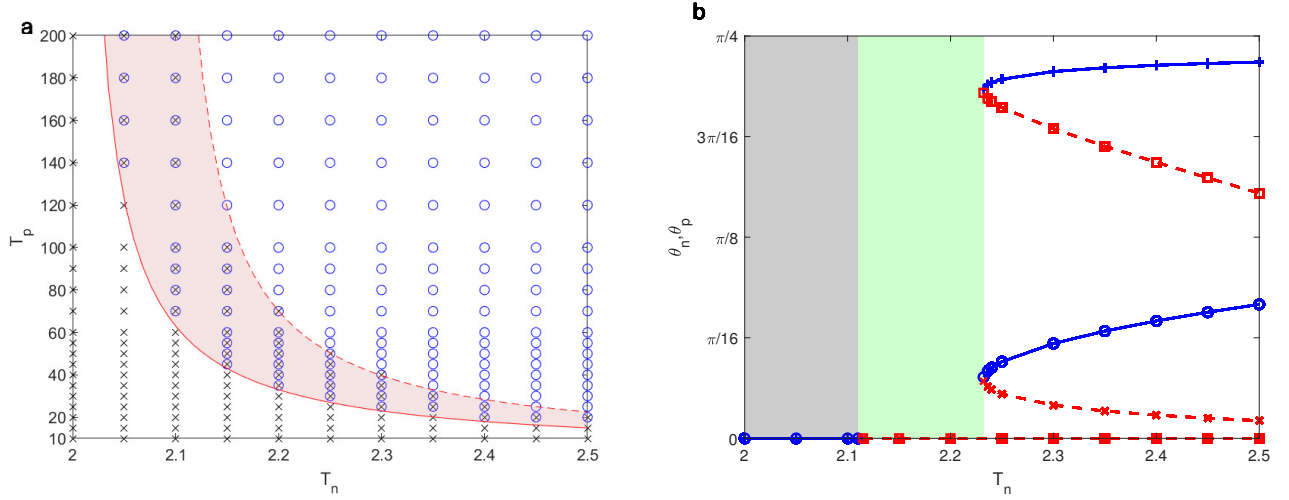


FIG. 1: (a) Phase diagram in the T_p - T_n space for $\lambda_n = \lambda_p = \nu = 1$. Crosses (\times) denote the region where the only fixed point is the trivial one, whether stable or unstable. Circles (\circ) denote the region where the trivial fixed point is unstable. The red shaded region is where oscillations occur. The solid red line is $T_p = 3T_n/(T_n - 2)$ and the dashed line is a numerical estimate of the second border of the oscillatory region. (b) Bifurcation diagram showing θ_n, θ_p as a function of T_n , with $T_p = 60$. Stable points are denoted by circles (+ marks) in blue and unstable points are denoted by cross (square) marks in red. The gray-shaded region ($T_n \lesssim 2.11$) is where the trivial fixed point is stable, green is where oscillatory behavior occurs, and the white region ($T_n \gtrsim 2.23$) is where more than one fixed point is present. The fixed points with negative values of θ_n, θ_p will be a reflection of the current figure with respect to the axis.

From Eqs. (4), it is easy to see that the active timescale modulates the speed of the evolution of the system towards any asymptotic limit, with larger t_a meaning slower dynamics.

To examine long-term dynamics, a linear stability analysis is performed by examining at any fixed point (θ_n^*, θ_p^*) the eigenvalues $e_i = (\text{Tr } J \pm \sqrt{(\text{Tr } J)^2 - 4 \text{Det } J})/2$, where $J_{ij} = \partial f_i / \partial \theta_j$ is the Jacobian. The origin $(0, 0)$ is a trivial fixed point for all values of the parameters, and a short calculation shows that a necessary condition for stability is $\text{Tr } J = \frac{\lambda_n}{2} - \frac{1}{T_n} - \frac{\lambda_p \nu_p}{2\nu T_p} - \frac{1}{T_p} < 0$. For simplicity, we assume $\lambda_n = \lambda_p = \nu = \nu_p = 1$ for the rest of this work. The condition for stability then simplifies to $T_p < 3T_n/(T_n - 2)$.

Thus any trajectory that begins in the neighborhood of the origin either asymptotically approaches this point if it is stable, or wanders away from it if $\text{Tr } J > 0$. This is indeed the case, as is illustrated in a typical phase diagram in Fig. 1a, where the red solid line gives the line $T_p = 3T_n/(T_n - 2)$ and the blue circles above it denote the region where a trajectory is *not* attracted to the trivial fixed point. If the trivial fixed point is attractive (points below the red line), the angles θ_n, θ_p asymptotically align towards 0, possibly in an oscillatory motion. Physically speaking, small values of either T_n or T_p imply rapid orientational relaxation dominating over the active forces.

Aside from the trivial fixed point, the mix of algebraic and transcendental functions in \mathbf{f} prevents us from analytically obtaining other fixed points, unlike other relaxation oscillators in literature (e.g. the Van der Pol equation)[28]. We thus approach the problem numerically and obtain both the location and the stability of any other fixed points of this system, as demonstrated in the bifurcation diagram in Fig. 1b. To obtain this diagram trajectories were initiated within the entire space and allowed to evolve until convergence to unique fixed points. In fact the locations of these fixed points can be anticipated by drawing the nullclines $\dot{\theta}_n = \dot{\theta}_p = 0$ for different values of the parameters and dimensionless values. A similar diagram can be constructed for when the bifurcation parameter is T_p .

There are three distinct regions in this figure. The first region, when the dimensionless nematic relaxation time, T_n , is sufficiently small (gray region), corresponds to when the trivial fixed point is stable. Here there are no other fixed points, and the origin provides the global attracting point of the system. The trivial fixed point loses its stability with increasing T_n . By contrast, if T_n is sufficiently large (white region), a saddle node bifurcation occurs at the intersection of the nullclines $\dot{\theta}_n = \dot{\theta}_p = 0$ and spontaneously gives birth to a pair of stable and unstable nodes [28]. The stable node approaches $(\pm\pi/4, \pm\pi/4)$ as $T_n \rightarrow \infty$, as expected from our earlier arguments.

For a narrow intermediate range of the dimensionless number T_n (the green region) the only fixed point is that at the origin, which is now unstable. We show that in this region the dynamical system undergoes an oscillatory motion in the nematic and polymer alignment angles θ_n, θ_p . To do this, we will utilize the Poincaré-Bendixson Theorem [28, 29], which can be invoked given a two-dimensional, continuously differentiable differential equation defined on an open set encompassing a compact subset Ω^* that contains a trajectory confined within Ω^* . The Poincaré-Bendixson Theorem asserts that if Ω^* does not contain any fixed points, then Ω^* contains a closed orbit. In our case, this closed orbit

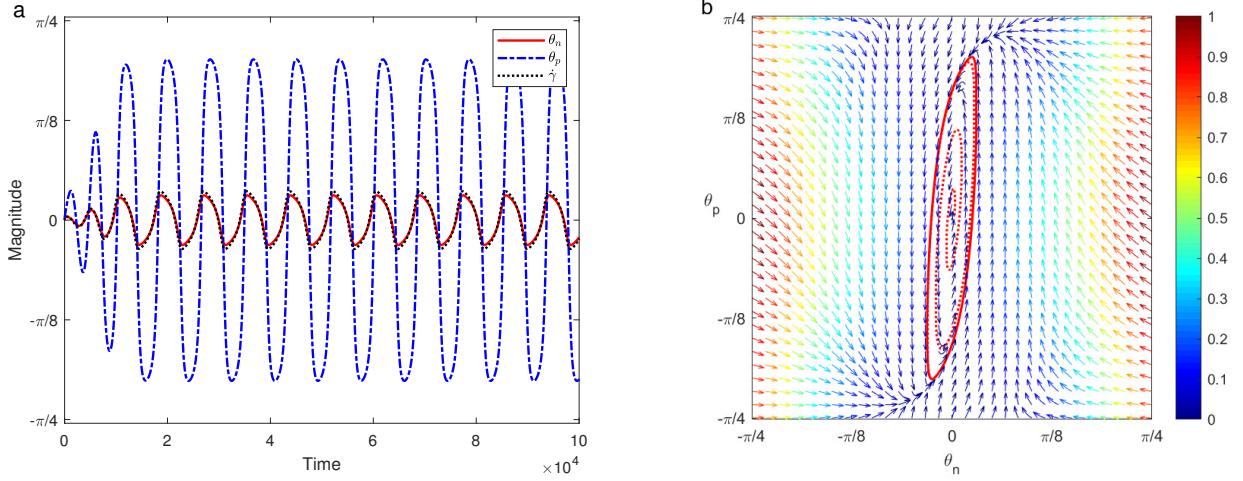


FIG. 2: (a) Time series displaying oscillatory motion for $T_n = 2.2, T_p = 60, t_a = 40$. (b) Corresponding vector plot and trajectory (red dotted line) of Eqs. (4) in the θ_n - θ_p space. Note that the vectors in the figure are rescaled to the maximum magnitude in the plot using the Matlab visualization package Streak [30].

corresponds to an oscillatory motion in the time evolution of the angles.

Note that the f_i as defined in Eqs. (4) are continuous in $\mathbb{R}^2 \supset \Omega$ and it can be easily shown (see Appendix) that Ω is a trapping region, i.e. all trajectories at the boundary point towards the interior of Ω , confining all trajectories within Ω . By erecting a small neighborhood \mathcal{B} of radius ϵ around the repeller $(0, 0)$, then $\Omega^* = \Omega \setminus \mathcal{B}(0; \epsilon)$ is a compact trapping region. As a consequence of the Poincaré-Bendixson Theorem, there is a closed orbit in this region, which implies oscillatory motion in θ_n, θ_p , as exemplified in the time series in Fig. 2a and the red orbit in Fig. 2b. The vector field in this figure further supports the attractive nature of this limit cycle.

Note that the bifurcation diagram in Fig. 1b is simply a slice of the red region in the full phase diagram in Fig. 1a, taken at a dimensionless polymer relaxation time, $T_p = 60$. Indeed it is in this red region of the phase diagram, corresponding to only one fixed point which is unstable, where the conditions of the Poincaré-Bendixson Theorem are satisfied. The transition from an attractive fixed point into a limit cycle shows that the curve $T_p = 3T_n/(T_n - 2)$ marks a supercritical Hopf bifurcation.

B. Fixed elastic modulus A_p

Next we study the case with fixed elastic modulus $A_p = \nu_p/t_p$. In contrast to the Eqs. (4) above, the dimensionless relaxation variable T_p ceases to appear in the shear terms, and there is a less simple dependence on the active timescale t_a . In this case, Eqs. (1)-(3) become

$$\dot{\theta}_n = \frac{1}{t_a} \left(\frac{\lambda_n}{4} \cos 2\theta_n \sin 2\theta_n - \frac{\lambda_n A_p t_a}{4\nu} \cos 2\theta_n \sin 2\theta_p - \frac{\theta_n}{T_n} \right), \quad (5a)$$

$$\dot{\theta}_p = \frac{1}{t_a} \left(\frac{\lambda_p}{4} \cos 2\theta_p \sin 2\theta_n - \frac{\lambda_p A_p t_a}{4\nu} \cos 2\theta_p \sin 2\theta_p - \frac{\theta_p}{T_p} \right). \quad (5b)$$

As in the previous case of constant polymer viscosity, the origin is a fixed point for all values of T_n, T_p . However, in the limit of vanishing relaxation $T_n, T_p \rightarrow \infty$, all the points in the curve $4\dot{\gamma} = \sin 2\theta_n - A_p \sin 2\theta_p/\nu = 0$ are fixed points of the system, and the domain to be considered cannot a priori be limited to Ω . Nevertheless, in the finite T_n, T_p case, it will be possible to restrict the analysis to Ω and to prove that oscillatory motion may still occur.

Performing the same stability analysis at the origin (with finite T_n, T_p), we now require two necessary conditions to establish stability: $\text{Tr } J < 0$ and $\text{Det } J > 0$, which are both dependent on the values of A_p and t_a . As before $0 > \text{Tr } J = \frac{\lambda_n}{2} - \frac{1}{T_n} - \frac{\lambda_p A_p t_a}{2\nu} - \frac{1}{T_p}$ which simplifies to $\frac{1}{T_n} + \frac{1}{T_p} > \frac{1 - A_p t_a}{2}$ if $\lambda_n = \lambda_p = \nu = 1$. Note that if $A_p t_a \geq 1$, the origin remains stable for all values of T_n, T_p , which implies that either the elastic modulus or the active time scale (or both) must be small to ensure stability. The other necessary condition for stability ($\text{Det } J > 0$), for the case $\lambda_n = \lambda_p = \nu = 1$, and under the assumption that $T_n > 2$, is $T_p > \frac{T_n - 2}{A_p t_a}$. This condition is shown as a pink line in

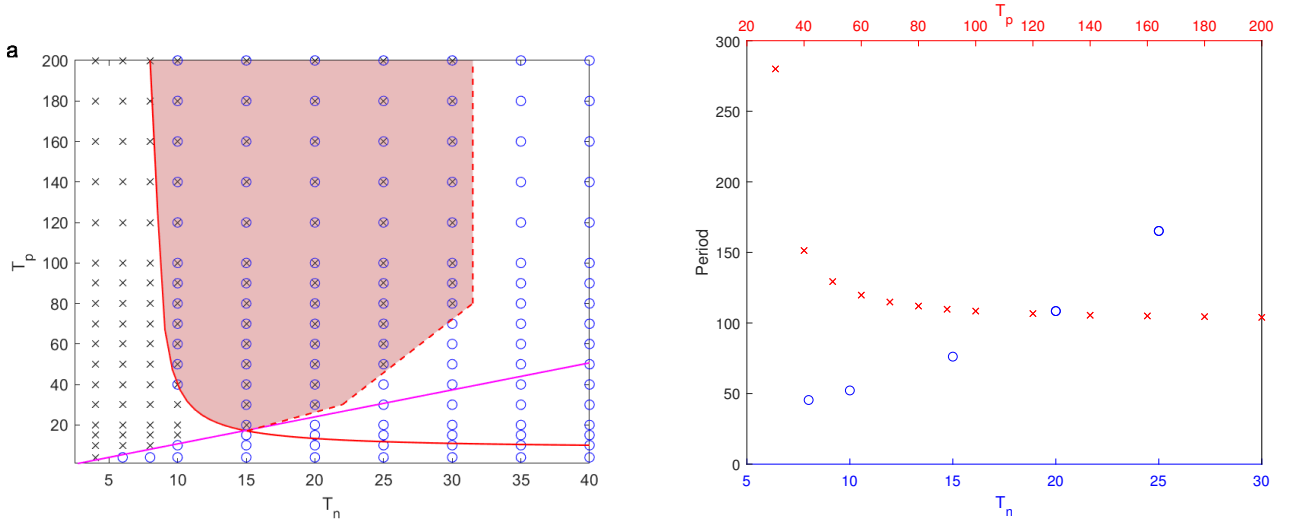


FIG. 3: (a) Phase diagram for $A_p = 0.5, t_a = 1.5$ for $\lambda_n = \lambda_p = \nu = 1$. The red curve is $\text{Tr } J = 0$ and the pink curve is $\text{Det } J = 0$. Crosses (\times) denote the region where the only fixed point is the trivial one, whether stable or unstable. Circles (\circ) denote the region where the trivial fixed point is unstable. The red shaded region is where oscillations occur. The dashed line is an approximate estimate of the boundary demarcating the region displaying oscillations. (b) The oscillation period for the active time scale $t_a = 1.5$ as a function of T_n (blue, with $T_p = 100$) or T_p (red, with $T_n = 20$).

Fig. 3 in a typical T_n - T_p phase space when $A_p t_a < 1$. Together the conditions now clearly dictate the boundary of the stable region.

We numerically explore different combinations of $A_p t_a$ and confirm that attractive orbits still exist as was found in the fixed ν_p case. As before, oscillations occur when the trivial fixed point is unstable and when no other singularity is present in the domain Ω , as seen in the typical phase diagram for $A_p t_a < 1$ in Fig. 3, although oscillations are observed for a possibly wider range $k_1 < T_n < k_2$, where k_1, k_2 are dependent on $A_p t_a$. The nematic relaxation t_n must remain sufficiently longer than t_a , else the activity-induced shear dominates suppressing the oscillations. The values of T_p that permit oscillations, in contrast to the fixed polymer viscosity case, can be much larger, owing to the fact that polymer stress in Eq. (3) is now independent of T_p .

Note that it would not be possible to guarantee a trapping region in the entire domain of θ_n, θ_p , and the presence of several fixed points will anyway prevent the use of the Poincaré-Bendixson Theorem. However the Poincaré-Bendixson Theorem can again be used if we restrict the initial conditions to a smaller domain, e.g. to Ω . The resulting vector diagrams and bifurcation diagrams are similar to the previous case. We also note that oscillations occur right before the bifurcations appear *spontaneously* in the bifurcation diagram, rather than the origin *splitting* into a pair of fixed points. The calculations to establish the trapping region, needed to utilise the Poincaré-Bendixson Theorem, are exactly the same as in the previous case, thanks to the same terms vanishing.

C. Periodicity

Previous models and experiments have shown that the oscillations of active matter in viscoelastic environments exhibit non-sinusoidal trajectories, consistent with the behaviour of dynamical systems as they move farther from a bifurcation point [23]. Here we characterize the oscillatory motion of our model and confirm that a similar behaviour can be observed for the periodicity and the shape of the orbits for different values of T_n and T_p .

We first report results for fixed polymer viscosity. The period of the oscillatory behavior, calculated numerically, increases nonlinearly as either T_n and T_p increases (Fig. 4a). The active timescale t_a simply rescales the period for a fixed T_n - T_p pair, as evidenced by the perfect collapse of the measured periods. As expected, the increase in the period is accompanied by a decreasingly sinusoidal shape in the time series of the angles. For instance, the insets at the top and bottom of Fig. 4b illustrate the evolution of the nematic alignment angle θ_n for identical values of T_n . The blue curve ($T_p = 50$) is barely indistinguishable from a sinusoidal curve whereas the red curve ($T_p = 70$) is reminiscent of the Fitzhugh-Nagumo or the Van der Pol oscillators, which are characterised by alternating slow-fast relaxation [28, 31].

To quantify the deviation of these trajectories from a sinusoid, we numerically calculate their Fourier spectra and

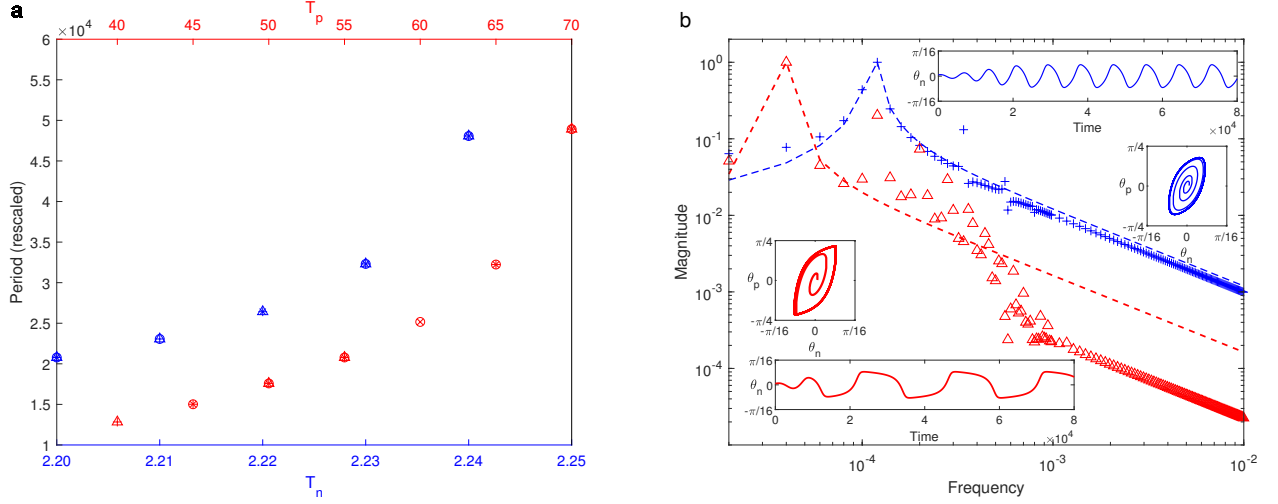


FIG. 4: (a) The oscillation period for the fixed polymer viscosity case, with active time scale $t_a = 120$ and as a function of T_n (blue, with $T_p = 55$) or T_p (red, with $T_n = 2.2$), obtained by rescaling simulations from $t_a = 20$ (Δ), $t_a = 30$ ($+$), $t_a = 40$ (\times), $t_a = 60$ (\circ). (b) Points indicate the normalized discrete Fourier transform of θ_n as a function of frequency; the dashed lines show the sinusoidal signal of corresponding periodicity (with an exponential tail arising from the numerical approximation). The parameters are $t_a = 60$, $T_n = 2.2$ and $T_p = 50$ (blue $+$), and $T_p = 70$ (red Δ), and the values are normalized for each case by the maximum value of the signal. The insets indicate the corresponding time series of θ_n and orbits in the θ_n - θ_p space.

compare them to the spectra of sinusoids with corresponding periods (Fig. 4b), with the peak in the frequencies indicating the inverse of the period. Oscillations that result from Eqs. (4) (in markers) indicate that the frequency distributions differ from the discretized sinusoidal counterparts (dashed lines) with more significantly-activated frequencies as T_p or T_n increases. This irregularity can be visually corroborated by looking at the orbits in the θ_n - θ_p phase space as provided in the accompanying insets. A sinusoidal trajectory would correspond to an elliptical shape, whereas the slow-fast dynamics manifests as a rugby-ball-shaped orbit, with nearly pointed tips. Moreover, we remark that the behaviour is closer to sinusoidal for pairs T_n - T_p near to the supercritical Hopf bifurcation (where $\text{Tr } J = 0$, red solid line in Fig. 1a), consistent with the findings in [23].

For the case of fixed elastic modulus, similar non-sinusoidal orbits are observed. While the period increases with T_n like in the fixed ν_p case, it however decreases with T_p and approaches a fixed value in this case (Fig. 3b). This asymptotic decrease in period is attributed to the polymer orientation being dominated by the fluctuating shear, which is independent of T_p in the fixed elastic modulus case. Slower polymer relaxation results in the slow-fast transition being attained faster.

IV. CONCLUSION

Our results help to elucidate the physics that underlies the existence of oscillatory dynamics. We first note that our minimal model of an active viscoelastic fluid displays oscillatory behavior when $T_n < T_p$. As such, the nematic director relaxes and seemingly equilibrates faster than the polymer, but polymer orientation attains larger values because of the stronger tendency to align to the shear (weaker relaxation term). Since the shear rate is an intricate balance between the active and polymeric stresses, then as the nematic angle approaches its (non-interacting) steady state, it gets pushed away from this *equilibrium* by feedback arising from the slower but stronger polymer force. Indeed, if θ_p is sufficiently larger than θ_n , then $\sin 2\theta_p > (T_p \nu / \nu_p) \sin 2\theta_n$ (for fixed polymer viscosity, ν_p) or $\sin 2\theta_p > (\nu / A_p t_a) \sin 2\theta_n$ (for fixed elastic modulus, A_p) thereby creating a polymeric stress large enough to flip the sign of the shear, $\dot{\gamma}$. The nematic angle θ_n then starts to realign to the new direction and overshoots beyond 0, flipping the sign of the active stress and the intensifying the shear rate in that opposite direction, resulting in a slow-fast dynamics.

To summarise, in this paper, we show how the viscoelastic components of a fluid can feedback on the shear flow generated by an active component and result in self-sustained oscillatory dynamics. The oscillations occur for specific ranges of dimensionless numbers relating the relaxation timescales of the active and viscoelastic components with the active timescale. In this range of values, linear stability analysis shows that the trivial fixed point of the system loses its stability, while numerical simulations verify that no other fixed point exists in the domain spanned by the orientation angles of the nematic and polymer, θ_n and θ_p , respectively. Whether the polymer viscosity or the elastic

modulus is fixed, the Poincaré-Bendixson Theorem can then be used to establish the existence of a limit cycle in (a subset of) the two-dimensional phase plane and, consequently, the oscillatory behavior in the shear rate and flow direction. For the case where the elastic modulus A_p is kept constant, further restrictions on the value of the product $A_p t_a$ are necessary to observe the oscillatory motion. The period for a full cycle increases and the oscillations become less sinusoidal as either the nematic or the polymer relaxation becomes slower. A slow-fast dynamics is observed, with the faster dynamics occurring once θ_n has flipped its orientation with respect to its equilibrium position. The physical mechanism behind this phenomenon is explained by considering the relative contributions of the active and polymeric stresses to the shear rate. We emphasize that the nonlinearity in the model does not result in any known oscillator models when truncated at any specific order.

Oscillatory dynamics is ubiquitous in biological systems, from simple predator-prey models to the more complex descriptions of how neurons transmit electrical signal spikes, such as the Hodgkin-Huxley model or its two-dimensional counterpart, the Fitzhugh-Nagumo model [31, 32]. Indeed, recently, a sustained oscillatory behavior of bacteria in a viscoelastic fluid was reported and studied using both a full hydrodynamic active viscoelastic model [23], and the Fitzhugh-Nagumo oscillator. Our two-dimensional model, motivated by concepts from sheared active nematics and in spite of only accounting for rotational relaxation and activity, captures the essential ingredients that will result in oscillatory behaviour: activity to generate a spontaneous flow and viscoelasticity that will generate sufficient amount of feedback. Our study thereby may provide a minimal framework to predict and analyze generic dynamical properties of biological systems, particularly those involving nematic active matter in a complex environment.

ACKNOWLEDGEMENTS

A. D. acknowledges funding from the Novo Nordisk Foundation (Grant no. NNF18SA0035142), Villum Fonden (Grant no. 29476), and European Union's Horizon 2020 research and innovation program under the Marie Skłodowska-Curie grant agreement No. 847523 (INTERACTIONS).

COMPETING INTERESTS

The authors declare no competing interests.

AUTHORS CONTRIBUTION

ELCMP, AD, and JMY conceptualized the study. ELCMP and HLT performed the analyses and simulations. All authors participated the preparation and submission of the manuscript.

VERIFICATION OF THE TRAPPING REGION

Consider the domain Ω and the vector field that arises from Eqs. (4). The following observations taken together mean that any trajectory beginning from the boundary remains confined within Ω .

- If $\theta_n = -\pi/4$, then, from Eq. 4a, $\cos 2\theta_n = 0$ so $\dot{\theta}_n = |\theta_n|/T_n > 0$. Any trajectory starting from the left side of the box Ω will point to the right.
- If $\theta_n = \pi/4$, then, from Eq. 4a, $\dot{\theta}_n = -\theta_n/T_n < 0$. Any trajectory starting from the right side of the box Ω will point to the left.
- If $\theta_p = -\pi/4$, then, from Eq. 4b, $\cos 2\theta_p = 0$ and so $\dot{\theta}_p = |\theta_p|/T_p > 0$. Any trajectory starting from the bottom side of the box Ω will point upwards.
- If $\theta_p = \pi/4$, then, from Eq. 4b, $\dot{\theta}_p = -\theta_p/T_p < 0$. Any trajectory starting from the top side of the box Ω will point downwards.

We further remark that the same analysis but using (5)a,b in the domain Ω results in the same observation that Ω is an external trapping region.

-
- [1] Marchetti M C, Joanny J F, Ramaswamy S, Liverpool T B, Prost J, Rao M, et al. 2013 Hydrodynamics of soft active matter *Reviews of Modern Physics* **85** 1143–1189
 - [2] Doostmohammadi A, Ignés-Mullol J, Yeomans J M, Sagués F 2018 Active nematics *Nature Communications* **9** 1–13
 - [3] Sanchez T, Chen D T N, DeCamp S J, Heymann M, Dogic Z 2012 Spontaneous motion in hierarchically assembled active matter *Nature* **491** 431
 - [4] Kumar N, Zhang R, de Pablo J J, Gardel M L 2018 Tunable structure and dynamics of active liquid crystals *Science Advances* **4** eaat7779
 - [5] Maroudas-Sacks Y, Garion L, Shani-Zerbib L, Livshits A, Braun E, Keren K 2020 Topological defects in the nematic order of actin fibres as organization centres of Hydra morphogenesis *Nature Physics* **17** 251–259
 - [6] Volfson D, Cookson S, Hasty J, Tsimring L S 2008 Biomechanical ordering of dense cell populations *Proceedings of the National Academy of Sciences* **105** 15346–15351
 - [7] Copenhagen K, Alert R, Wingreen N S, Shaevitz J W 2020 Topological defects promote layer formation in *Myxococcus xanthus* colonies. *Nature Physics* **17** 211–215
 - [8] Meacock O J, Doostmohammadi A, Foster K R, Yeomans J M, Durham W M 2020 Bacteria solve the problem of crowding by moving slowly *Nature Physics* **17** 205–210
 - [9] Duclos G, Blanch-Mercader C, Yashunsky V, Salbreux G, Joanny J F, Prost J, et al 2018 Spontaneous shear flow in confined cellular nematics *Nature Physics* **14** 728–732
 - [10] Kawaguchi K, Kageyama R, Sano M 2017 Topological defects control collective dynamics in neural progenitor cell cultures *Nature* **545** 327–331
 - [11] Saw T B, Doostmohammadi A, Nier V, Kocgozlu L, Thampi S, Toyama Y, et al. 2017 Topological defects in epithelia govern cell death and extrusion *Nature* **544** 212–216
 - [12] Blanch-Mercader C, Yashunsky V, Garcia S, Duclos G, Giomi L, Silberzan P 2018 Turbulent dynamics of epithelial cell cultures *Physical Review Letters* **120** 208101
 - [13] Nadell C D, Drescher K, Wingreen N S, Bassler B L 2015 Extracellular matrix structure governs invasion resistance in bacterial biofilms *The ISME Journal* **9** 1700–1709
 - [14] Hobley L, Harkins C, MacPhee C E, Stanley-Wall N R 2015 Giving structure to the biofilm matrix: an overview of individual strategies and emerging common themes *FEMS Microbiology Reviews* **39** 649–669
 - [15] Vidakovic L, Singh P K, Hartmann R, Nadell C D, Drescher K 2018 Dynamic biofilm architecture confers individual and collective mechanisms of viral protection *Nature Microbiology* **3** 26–31
 - [16] Carey S P, Martin K E, Reinhart-King C A 2017 Three-dimensional collagen matrix induces a mechanosensitive invasive epithelial phenotype *Scientific Reports* **7** 42088
 - [17] Mereness J A, Bhattacharya S, Wang Q, Ren Y, Pryhuber G S, Mariani T J 2018 Type VI collagen promotes lung epithelial cell spreading and wound-closure *PLOS ONE* **13** e0209095
 - [18] Chaudhuri O, Cooper-White J, Janmey P A, Mooney D J, Shenoy V B 2020 Effects of extracellular matrix viscoelasticity on cellular behaviour *Nature* **584** 535–546
 - [19] Fletcher D A, Mullins R D 2010 Cell mechanics and the cytoskeleton *Nature* **463** 485–492
 - [20] Pritchard R H, Huang Y Y S, Terentjev E M 2014 Mechanics of biological networks: from the cell cytoskeleton to connective tissue *Soft Matter* **10** 1864–1884
 - [21] Hemingway E J, Cates, E M, Fielding S M 2016 Viscoelastic and elastomeric active matter: Linear instability and nonlinear dynamics *Physical Reviews E* **93** 032702
 - [22] Plan E L C V M, Yeomans J M, Doostmohammadi A 2020 Active matter in a viscoelastic environment *Physical Review Fluids* **5** 023102
 - [23] Liu S, Shankar S, Marchetti M C, Wu Y 2021 Viscoelastic control of spatiotemporal order in bacterial active matter *Nature* **590** 80–84
 - [24] Plan E L C V M, Yeomans J M, Doostmohammadi A 2021 Activity pulses induce spontaneous flow reversals in viscoelastic environments *Journal of the Royal Society Interface* **18** 20210100
 - [25] Giomi L, Mahadevan L, Chakraborty B, Hagan M F 2011 Excitable Patterns in Active Nematics *Physical Review Letters* **106** 218101
 - [26] Woodhouse F G, Goldstein R E 2012 Spontaneous Circulation of Confined Active Suspensions *Physical Review Letters* **109** 168105
 - [27] Aigouy B, Farhadifar R, Staple D B, Sagner A, Röper JC, Jülicher F, et al. 2010 Cell flow reorients the axis of planar polarity in the wing epithelium of *Drosophila* *Cell* **142** 773–786
 - [28] Strogatz S H 1994 *Nonlinear Dynamics And Chaos: With Applications To Physics, Biology, Chemistry, And Engineering* (Massachusetts: Perseus Books)
 - [29] Perko L 2001 *Differential Equations and Dynamical Systems* (New York: Springer Verlag)
 - [30] Dano B 2021 StreakArrow. MATLAB Central File Exchange. Available from: <https://www.mathworks.com/matlabcentral/fileexchange/22269-streakarrow>

- [31] FitzHugh R 1955 Mathematical models of threshold phenomena in the nerve membrane *Bulletin of Mathematical Biophysics* **17** 257–278.
- [32] Hodgkin A L, Huxley A F 1952 Currents carried by sodium and potassium ions through the membrane of the giant axon of *Loligo* *The Journal of Physiology* **116** 449–472